OPEN

Alternative splicing contributes to the coordinated regulation of ferritin subunit levels in *Bactrocera dorsalis* (Hendel)

Xuan-Zhao Jiang, Lin Cong, Jin-Zhi Niu, Wei Dou & Jin-Jun Wang

Key Laboratory of Entomology and Pest Control Engineering, College of Plant Protection, Southwest University, Chongqing 400715, P. R. China.

A constant ratio of ferritin heavy chain homolog (HCH) and light chain homolog (LCH) subunits seems to be required to compose the ferritin heteropolymer protein in insects. However, the mechanism by which insect LCH genes regulate protein levels remains unclear. We report that alternative promoters and alternative splicing contribute to maintaining a constant ratio of the two subunits, BdFer1HCH and BdFer2LCH (ferritin 1 HCH and ferritin 2 LCH), in *Bactrocera dorsalis*, a notorious quarantine pest. The genes *BdFer1HCH* and *BdFer2LCH* were identified with a series of potential transcription factor binding sites and were shown to be clustered within the genome in a "head to head" fashion. Thus, we unearthed a potential post-transcriptional mechanism to regulate the levels of LCH subunits, and confirmed that the expressions of *BdFer1HCH* and *BdFer2LCH* were induced by 20-hydroecdysone, iron overload, and immune challenge.

I ron exhibits a dual nature in organisms, both as an indispensable micronutrient and a potent toxin. Organisms must intake adequate amounts of dietary iron for numerous physiological functions, such as respiration, nucleotide synthesis, steroid production and amino acid production[1]. At the same time, organisms must avoid the potential toxic properties of iron, which can cause oxidative damage to biomolecules[2,3]. To achieve iron homeostasis, organisms have evolved strategies to allow iron absorption and transport, but prevent the accumulation of redox-active iron in sensitive tissues[4]. In insects, ferritins are iron-binding proteins, similar to the function of transferrins, and play key roles in iron transport and storage[5]. Unlike mammalian ferritins, insect ferritins are mostly involved in the secretory pathways and circulate in the hemolymph[5], which is consistent with the fact that they are synthesized with a signal peptide, presumably directing the mature subunits to the secretory pathways. This kind of insect ferritin consists of two types of secretory subunits: a mammalian heavy chain homologue (HCH) that contains a ferroxidase center, and a mammalian light chain homologue (LCH) that facilitates the nucleation of the ferrihydrite iron core[6]. Insect *HCH* and *LCH* genes are reported to be arranged "head to head" and transcribed in opposite directions[7]. Such a structure is implicated in the coordinated regulation of ferritin at the transcriptional level[7], which is mediated by shared regulatory elements[8].

A post-transcriptional regulation mechanism mediated by the interaction of the iron responsive element (IRE) and iron regulatory protein (IRP) controls the synthesis of HCH subunits[5]. IRE is a stem-loop structure at the 5′ untranslated region (UTR) of ferritin messages. A genomic survey of ferritin reveals that almost all insect *HCH* genes have an IRE, while most of the *LCH* genes lack an IRE, except in Lepidoptera[5]. Recent research on *Drosophila melanogaster* ferritin (Fer1HCH and Fer2LCH) demonstrated that a constant ratio of the ferritin subunits is maintained *in vivo*; a protein degradation mechanism was proposed to regulate the level of the Fer2LCH subunit[9,10]. However, such a post-transcriptional mechanism remains to be clarified in insects.

In addition to its role in iron homeostasis[10], insect ferritin may have multiple functions, such as in cell proliferation, in embryonic and post-embryonic development, as a cytotoxic protector against oxidative stress and thermal stress, and as a potential antimicrobial effector[11–15]. Both subunits are critical for insect survival, and their deletion can lead to embryonic death and developmental arrest[9,16].

Given these differences from their mammalian homologues, insect ferritins are promising candidate targets for agricultural and medical pest control. *Bactrocera dorsalis* (Hendel) (Diptera: Tephritidae) is one of the most destructive and widespread polyphagous agricultural insect pests, feeding on more than 250 species of vegetables and fruits and causing severe economic losses each year[17]. Severe resistance in *B. dorsalis* populations greatly compromises the effects of chemical insecticides, gravely threatening the effective and sustainable usage of these
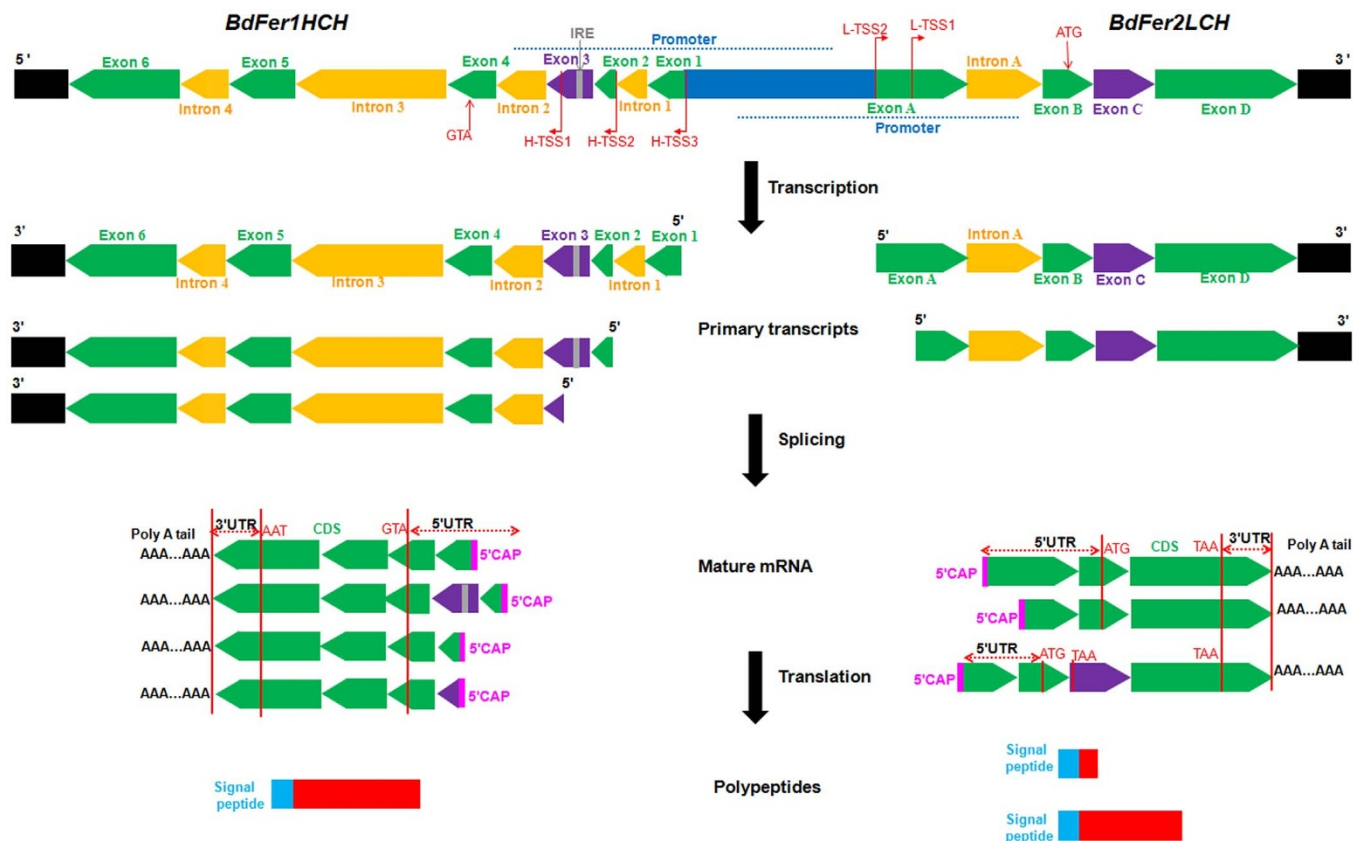
Figure 1 | Schematic representation of gene organization and expression patterns of *Bactrocera dorsalis* ferritin. Constitutive exons are shown as green blocks, alternatively spliced exons are shown as purple blocks, introns as yellow blocks, the intergenic regions as blue blocks, approximate promoter regions as blue dashed lines, other regulatory regions as black blocks, the IRE as a gray box, the 5′ cap as a purple box. The exons and introns of *BdFer1HCH* and *BdFer2LCH* are named using Arabic numerals and capital letters, respectively. The location of alternative TSSs is indicated using broken arrowed lines; the arrow indicates the direction of transcription. The location of start and stop codons are also shown. The UTR regions are indicated with double arrow lines. The 3′ UTR may vary for each transcript, although they are indicated using the same block. The poly(A) tails are also indicated. Putative signal peptides are shown as light blue boxes, and the mature polypeptides as red boxes. Locations and sizes are not to scale.

compounds[18]. Therefore, new, effective strategies are urgently needed, and study of the ferritin of *B. dorsalis* may help to develop such strategies.

This study shows that the post-transcriptional mechanism, intron retention, is possibly responsible for the regulation of LCH subunit levels by inducing a premature stop codon in the LCH transcripts, which leads to the generation of truncated proteins. A classic IRE is also identified at the HCH 5′ UTR of *B. dorsalis*, whose inclusion in the transcripts is coordinated by alternative transcription start sites (TSSs) and alternative splicing. Moreover, several potential functions for *B. dorsalis* ferritin are implicated by analyzing the genomic sequences and expression profiles resulting from abiotic and biotic stresses.

Results

Characterization of genomic sequences and cDNAs of *B. dorsalis* ferritin. *BdFer1HCH* (Ferritin 1 heavy chain homologue of *B. dorsalis*) and *BdFer2LCH* (Ferritin 2 light chain homologue of *B. dorsalis*) were clustered in the genome in a "head to head" fashion (Fig. 1 and Supplementary Fig. 1). Three TSSs, designated H-TSS1, H-TSS2, and H-TSS3, existed in the gene *BdFer1HCH*, among which H-TSS1 and H-TSS2 were identified by 5′ RACE, while the precise location of H-TSS3 was not determined. At least three primary transcripts were generated, which were further spliced into four types of mRNAs despite the presence of alternative polyadenylation sites (Fig. 1). An alternatively spliced exon named exon 3 was identified at the 5′ UTR between H-TSS1 and H-TSS2 (Fig. 1 and

Supplementary Fig. 1). A consensus sequence, acting as IRE required for post-transcriptional regulation, was identified in exon 3. Furthermore, two potential RNA editing sites, including a U to C and a C to U, were identified in the IRE (Supplementary Fig. 2A) by sequencing multiple clones. Several potential polyadenylation sites were predicted, whereas only one for *BdFer1HCH* was confirmed by 3′ RACE. However, all *BdFer1HCH* mRNAs encoded a 204-residue polypeptide (GenBank accession number: KF499586) with a putative membrane targeting signal of 17 amino acid residues at the N-terminus (Supplementary Fig. 1). The BdFer1HCH subunit preserved all seven conserved amino acid residues forming the ferroxidase center (Supplementary Fig. 1). One putative N-linked glycosylation site (N-X-S/T) was present at its N-terminus (Supplementary Fig. 1 and 2B).

For *BdFer2LCH*, two types of primary transcripts were detected; they resulted from two alternative TSSs, termed L-TSS1 and L-TSS2 (Fig. 1). L-TSS1 was detected by 5′ RACE, while the exact location of L-TSS2 was not determined. No potential IRE was found at the 5′ UTR of *BdFer2LCH*. Of interest is that an alternatively spliced exon C, generated by intron retention, was found in the coding region (Fig. 1). Nevertheless, a premature stop codon was introduced when the alternative exon C was spliced into the transcripts. Therefore, at least three types of mRNAs were generated because of the alternative TSSs and alternative splicing. Additionally, at least two polyadenylation sites existed for *BdFer2LCH* as shown in Supplementary Fig. 1. The ORF of *BdFer2LCH*, excluding exon C (GenBank accession number: KF499587), encoded a 223 amino-acid polypeptide. The
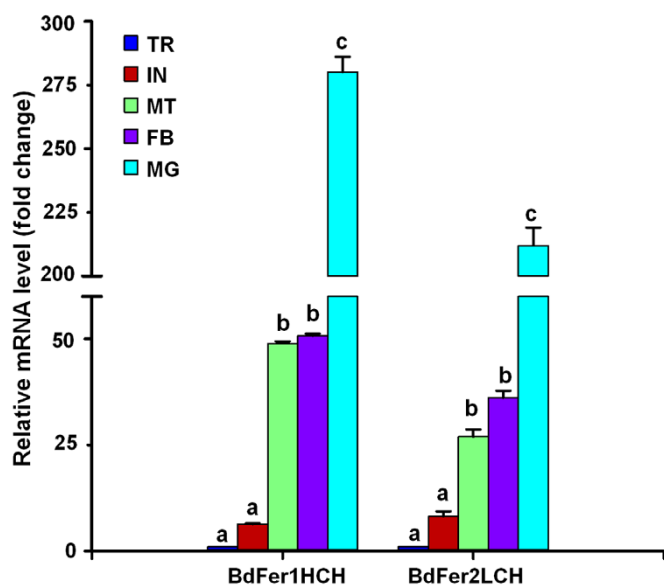
Figure 2 | Tissue transcription profiling of *Bactrocera dorsalis ferritin* in larvae. RT-qPCR analysis of the relative expression levels in five larval tissues: the fat body (FB), integument (IN), midgut (MG), Malpighian tubules (MT), and trachea (TR). All values are normalized relative to the expression levels in trachea (set as 1). Data are mean $2^{-\Delta\Delta Ct}$ values of three independent biological replicates ± SEM. Differences were analyzed by one-way ANOVA. In all cases, bars denoted with different letters had significant differences ($p < 0.05$, Tukey HSD's test).

deduced amino acid sequence was synthesized with a leading signal peptide consisting of 21 amino acid residues (Fig. 1). Like its insect homologues, BdFer2LCH lacked most of the amino acids forming the ferroxidase center (Supplementary Fig. 1 and 2B). A putative N-linked glycosylation site was present at its N-terminus. The truncated protein was composed of 39 amino acid residues.

Analyses of the upstream regions for putative transcription factor binding sites (TFBSs). We analyzed the control regions (2000-nucleotide regions upstream of the start codons) of *BdFer1HCH* and *BdFer2LCH* to identify putative Nuclear Factor-kappaB (NF-kappaB) and Broad-Complex (BR-C) binding sites as well as putative TFBSs located within the ±50-nucleotide regions around the TSSs. The results showed that no NF-κB was found within the sequences between the start codons of *BdFer1HCH* and *BdFer2LCH*. Consequently, we further analyzed the first intron sequence downstream from the start codon, revealing the presence of three NF-kappaBs (Supplementary Fig. 1). A total of 11 putative BR-C binding sites were predicted, including two BR-C Z1, four BR-C Z3, and five BR-C Z4 binding sites (Supplementary Fig. 1). The TFBSs within the ±50-nucleotide regions around the TSSs, which might be part of the core promoter, were predicted by AliBaba 2.1. Nine putative TFBSs were identified along H-TSS1, including C/EBP (CCAAT/enhancer-binding protein), NF-1 (Neurofibromatosis 1), Pit-1a (pituitary-specific positive transcription factor-1a), HNF-1 (hepatocyte nuclear factor-1), GR (Glucocorticoid receptor), Oct-1 (octamer binding protein 1), Sp1 (specificity protein 1), and TBP (TATA-binding protein) sites (Supplementary Fig. 1). The initiator element (Inr) overlapping the H-TSS1 was 5′-TCA$_{+1}$GATC-3′, in agreement with the consensus sequence 5′-PyPyA$_{+1}$NT/APyPy-3′. A canonical TATA box, 5′-TATAAAG-3′ (consensus sequence: 5′-TATAWAW-3′) was located 27 nucleotides upstream from the H-TSS1. Eight TFBSs were identified along H-TSS2, including Sp1, CREB (cAMP response element-binding protein), Oct-1, AP-1 (activator protein 1), TBP, C/EBP, and GATA-1 (GATA-binding protein 1). The corresponding Inr sequence was 5′-TCA$_{+1}$GTAC-

3′, where a purine A$_{+4}$ replaced the pyrimidine. At position −26 to −33 nucleotides upstream from the H-TSS2 lay a non-canonical TATA box (5′-TTTAAAA-3′) (Supplementary Fig. 1). Six putative TFBSs were identified around L-TSS1, including C/EBP, ICSBP (interferon consensus sequence binding protein), Oct-1, TBP, GATA-1, and HNF-3 (hepatocyte nuclear factor 3) (Supplementary Fig. 1). A non-canonical Inr (5′-TCA$_{+1}$TTGA-3′) corresponded to L-TSS1, and the upstream sequence 5′-TATAAGC-3′ (−23 to −29 nucleotides) might be recognized as a non-canonical TATA box. Additionally, a TATA box consensus sequence (5′-TATAAAA-3′) was present downstream at position +26 to +33 nucleotides.

Tissue and developmental transcription profiling of *B. dorsalis* ferritin. The primers used in RT-qPCR and RT-PCR analysis for *BdFer1HCH* and *BdFer2LCH* were designed to anneal to the common regions so that we could detect the abundances of all variants. The expression of *BdFer1HCH* was detectable in all tested larval and adult tissues (Fig. 2 and Fig. 3A). The highest expression was observed in the midgut, followed by the fat body, Malpighian tubules, integument, and trachea in larvae (Fig. 2). In adults, relatively high expression was also detected in the midgut and fat body, while relatively low expression was observed in the ovary (Fig. 3A). Several variants of both *BdFer1HCH* and *BdFer2LCH* were also detected in adult tissues. The product H3 was amplified using a sense primer located upstream from H-TSS2 and an antisense primer located downstream of the start codon; it represented the abundance of the variant initiating with H-TSS3. When the transcripts initiated with H-TSS3, the sequencing results indicated that intron 1, exon 2, exon 3 and intron 2 were spliced out as parts of an intron (Fig. 1). The variants initiating with H-TSS3 had relatively low expression in all nine tested adult tissues. The product H2 represented the variants initiating with H-TSS2, which were amplified using a sense primer located between H-TSS1 and H-TSS2 and an antisense primer located downstream the start codon. Two variants were observed that initiated with H-TSS2 and were due to alternative splicing (Fig. 3A). Further sequencing analysis revealed that exon 3 was alternatively spliced. The two variants also had a wide distribution in all tested adult tissues (Fig. 3A). The midgut and ovary contained a high abundance of the variant with exon 3 included, while other tissues seemed to have a similar distribution of the two variants (Fig. 3A). The developmental expression profiling showed that *BdFer1HCH* had the lowest expression in eggs, the highest in larvae, and a wide distribution in all stages (Supplementary Fig. 3). The splicing variants seemed to have stage-specific expression. In eggs, only the variant including exon 3 was observed. In the larvae and both male and female adults, the variant including exon 3 was the main mRNA type, whereas in pupae the expression levels of both variants were similar (Fig. 3C).

BdFer2LCH was very similar to *BdFer1HCH* in its tissue and developmental expression profiling; however, the expression of *BdFer2LCH* dominated at the adult stage (Supplementary Fig. 3). Three variants were observed for *BdFer2LCH*, as illustrated by the products, BdFer2LCH and L2 (Fig. 3A). L2 was amplified using a sense primer upstream of L-TSS1 and an antisense primer downstream of the start codon to selectively target the variant initiating with L-TSS2. This variant had relatively low expression in all adult tissues except the head (Fig. 3A). The product, BdFer2LCH, which was amplified using a sense primer downstream from L-TSS1 and an antisense primer near the stop codon, had two variants, either with or without exon C as a result of alternative splicing (Fig. 3A). The variant including exon 3 seemed to mainly express in the ovary. To better discern the splicing variants, we amplified the product BdFer2LCH′ (Fig. 3B), which was part of BdFer2LCH but shorter, and spanned the region including exon C. Both variants were observed in all adult tissues, but the one excluding exon C dominated in all tissues (Fig. 3B). The variant
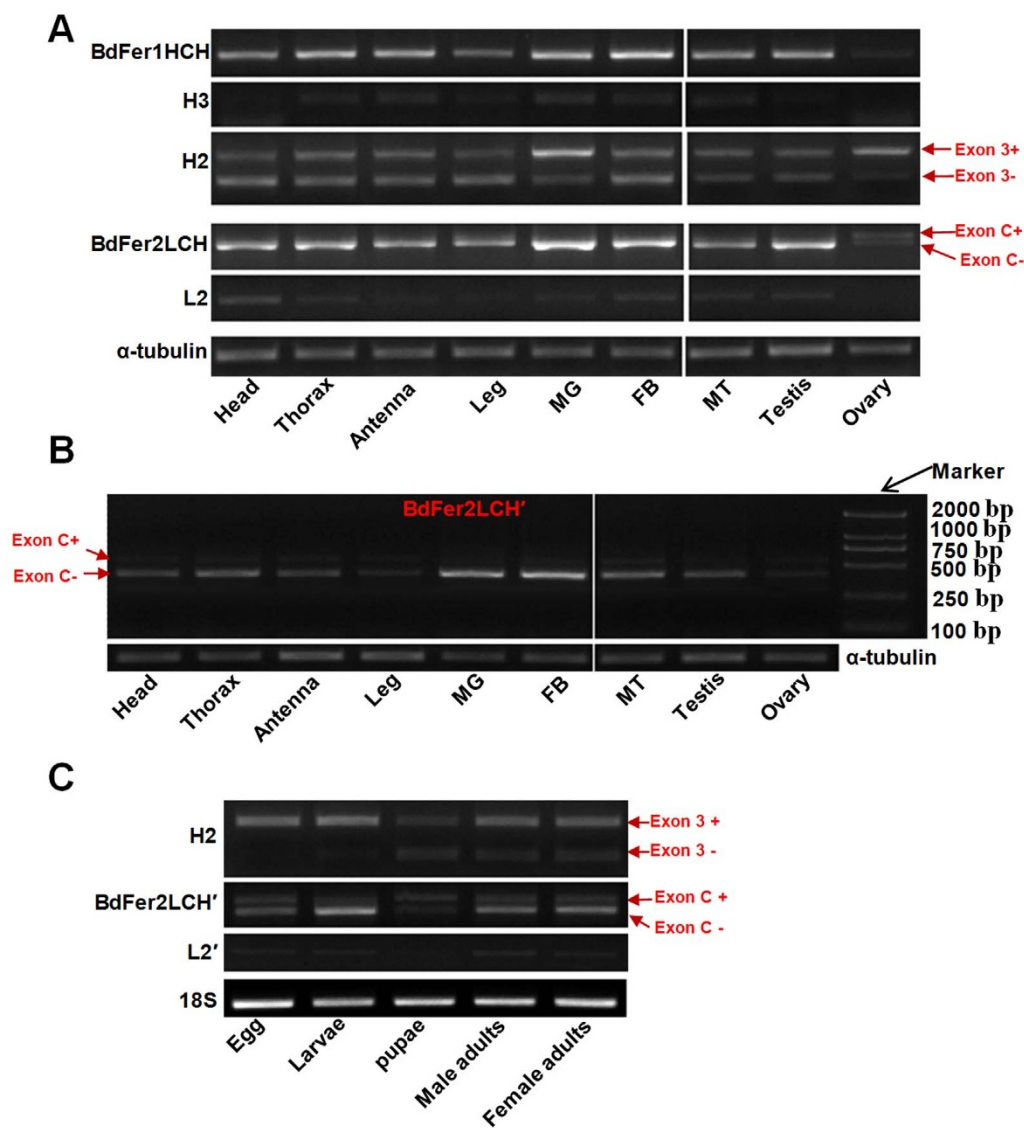
Figure 3 | RT-PCR assay of the expressions of splicing variants of *BdFer1HCH* and *BdFer2LCH* in adult tissues and developmental stages. (A) RT-PCR analysis of the expression levels of different variants in adult tissues. α-*tubulin* was the loading control to indicate equal amounts of RNA. The signs "+" and "−"indicate the inclusion or exclusion of alternative exons. The products BdFer1HCH and BdFer2LCH represent overall expression levels. H3 indicates the expression levels of variants initiating with H-TSS3; H2 indicates the expression levels of variants initiating with H-TSS2; L2 represents the expression levels of variants initiating with L-TSS2. (B) RT-PCR assay of the splicing variants of BdFer2LCH including or excluding exon C in adult tissues. The product BdFer2LCH′ in place of BdFer2LCH was used to make the bands more discernable. (C) RT-PCR assay of the splicing variants of *BdFer1HCH* and *BdFer2LCH* in different developmental stages. *18S ribosomal RNA* (18S) was used as the loading control. L2′ is used to indicate that no alternative splicing events occurred when the transcripts initiated with L-TSS2. All gels were run under the same conditions. Full-length gels are shown in the supplementary data section.

including exon C was also detected in all developmental stages, but the larvae seemed to mainly express the variant without exon C (Fig. 3C). To check whether the alternative splicing occurred when the transcript initiated with L-TSS2, the PCR product L2′ was generated using a sense primer upstream from L-TSS1 and an antisense primer downstream of exon C. Only a single product excluding exon C was amplified (Fig. 3C), which was further confirmed by sequencing multiple clones. Thus, exon C was induced only when the transcripts initiated with L-TSS1.

Iron overload dramatically altered the expression of *B. dorsalis* ferritin. The expressions of both *BdFer1HCH* and *BdFer2LCH* increased significantly 12, 24, and 36 h after the insect began feeding on an artificial diet supplemented with 1.8 mg/g $FeCl_3$, and the expressions of both genes peaked 24 h after feeding (Fig. 4A and

B). Moreover, larvae feeding on a diet supplemented with 1.8 mg/g $FeCl_3$ for 24 h gained significantly less weight than those eating diets supplemented with 0 mg/g and 0.18 mg/g $FeCl_3$ (Fig. 5A). However, both 0.18 mg/g and 1.8 mg/g $FeCl_3$ could significantly up-regulate the expressions of *BdFer1HCH* and *BdFer2LCH*, while no apparent dosage-effect was observed between the 0.18 mg/g and 1.8 mg/g treatments (Fig. 5B).

We further estimated the effects of iron overload on the expressions of *BdFer1HCH* and *BdFer2LCH* in the larval midgut and in the carcass without the midgut, because the midgut is the main organ responsible for iron absorption. The results showed that the expressions of *BdFer1HCH* and *BdFer2LCH* both increased in the larval midgut and carcass without midgut after feeding on the diet supplemented with $FeCl_3$ for 24 h (Fig. 5D). The variant excluding exon 3 was mainly detected in the carcass without midgut, and the variant
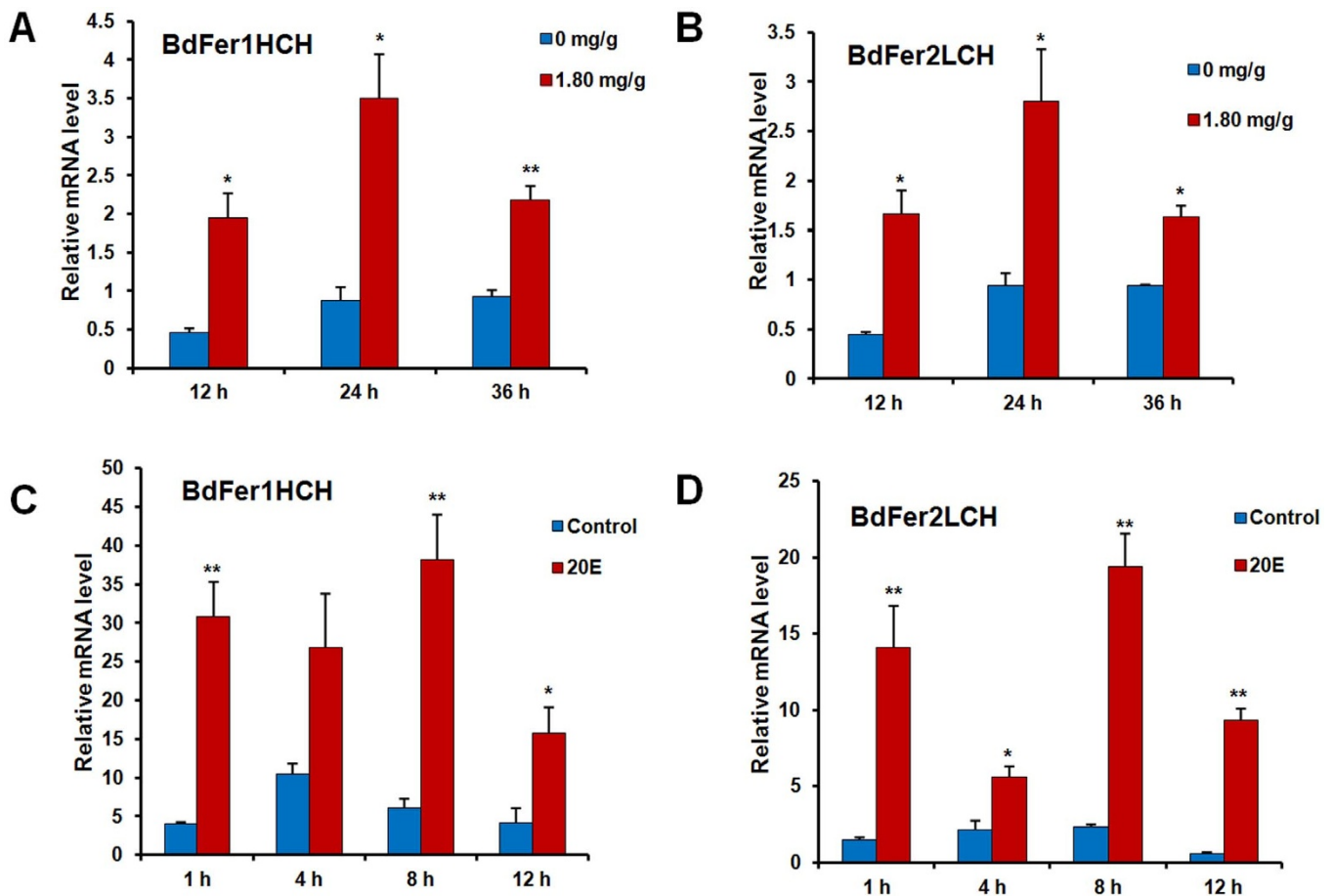
Figure 4 | Relative expression levels of *Bactrocera dorsalis* ferritin after iron overload and 20E injection. (A, B) Expression levels of *BdFer1HCH* and *BdFer2LCH* after a diet supplemented with 0 mg/g or 1.8 mg/g $FeCl_3$ for 12, 24, and 36 h. (C, D) Effect of 20-hydroxyecdysone (20E) on transcript abundances of *BdFer1HCH* and *BdFer2LCH* in third-instar larvae at 1, 4, 8, and 12 h post injection. All results are represented as mean $2^{-\Delta Ct}$ values of three independent biological replicates ± SEM. The two-tailed, unpaired t-test was used to test significance. Asterisks indicate significant differences in relative expression. (*, $p < 0.05$; **, $p < 0.01$).

including exon 3 was the main mRNA type in the midgut and in the carcass without midgut (Fig. 5C). Iron overload up-regulated the expression of the variant including exon 3, but had no apparent effect on the expression of the variant excluding exon 3. Similar expression levels in the midgut and carcass without midgut were observed for the variant initiated with H-TSS3, and the expression level increased in the midgut and carcass without midgut after iron overload (Fig. 5C). The transcript initiating with L-TSS2 represented by the product L2 was mainly expressed in the larval midgut. However, the expression level of the transcript initiating with L-TSS2 generally increased with an increasing dosage of iron (Fig. 5D).

Upregulation of *B. dorsalis* ferritin by exogenous 20E. *BdFer1HCH* and *BdFer2LCH* mRNAs were significantly increased after injection of 20-hydroxyecdysone (20E) at all four tested time points (Fig. 4C and D). The mRNA levels of *BdFer1HCH* had increased by more than 7-fold 1 h post injection. A more than 9-fold increase was observed for *BdFer2LCH* at 1 h post injection, and a greater increase up to 16-fold, had occurred 12 h post injection. The transcription patterns of *BdFer1HCH* and *BdFer2LCH* were very similar, but the response of *BdFer2LCH* was much more intense than that of *BdFer1HCH*.

Repressed expression of *B. dorsalis* ferritin by *E. coli*, PGN-SA, and PGN-SB. The antimicrobial peptide gene *diptericin* is sensitive to immune challenge. To ensure the effectiveness of the immune challenge, the expression patterns of the *diptericin* gene (GenBank

accession number: KJ488999) of *B. dorsalis* were used as an indicator. The expression of *diptericin* was up-regulated by injecting sterilized saline (insect physiological saline; 150 mM NaCl, 5 mM KCl, pH 6.8) or sterilized water and further induced by *E. coli*, PGN-SA (peptidoglycan from *Staphylococcus aureus*), and PGN-EB (peptidoglycan from *E. coli 0111:B4*), which suggested that an immune reaction was generated in *B. dorsalis* (Fig. 6A and D). Additionally, *diptericin* was induced more by *E. coli* and PGN-EB than by PGN-SA at 9 h post treatment (Fig. 6A and D). Therefore, these results validate the subsequent analysis of *B. dorsalis* ferritin.

BdFer1HCH was significantly induced by injection of saline compared with the control group at 6 h and 9 h post treatment, while *E. coli* had a slightly weaker effect than saline (Fig. 6B). BdFer1HCH was also up-regulated, compared with the control group, by injection of sterile water at 9 h post treatment, but was significantly repressed by PGN-SA and PGN-EB at 9 h compared with the water group (Fig. 6E). *BdFer2LCH* was also induced by sterilized saline in contrast to the control group at 3 h and 9 h, and was significantly depressed by *E. coli* at 9 h compared with that in the saline group (Fig. 6C). The expression of *BdFer2LCH* was significantly decreased by PGN-SA and PGN-EB at 3 h compared with that in the water group and was sustained at a relatively low level at 6 h and 9 h post injection (Fig. 6F).

Discussion
HCH and LCH are characterized by post-transcriptional regulatory mechanisms that are required to facilitate the balancing of subunit
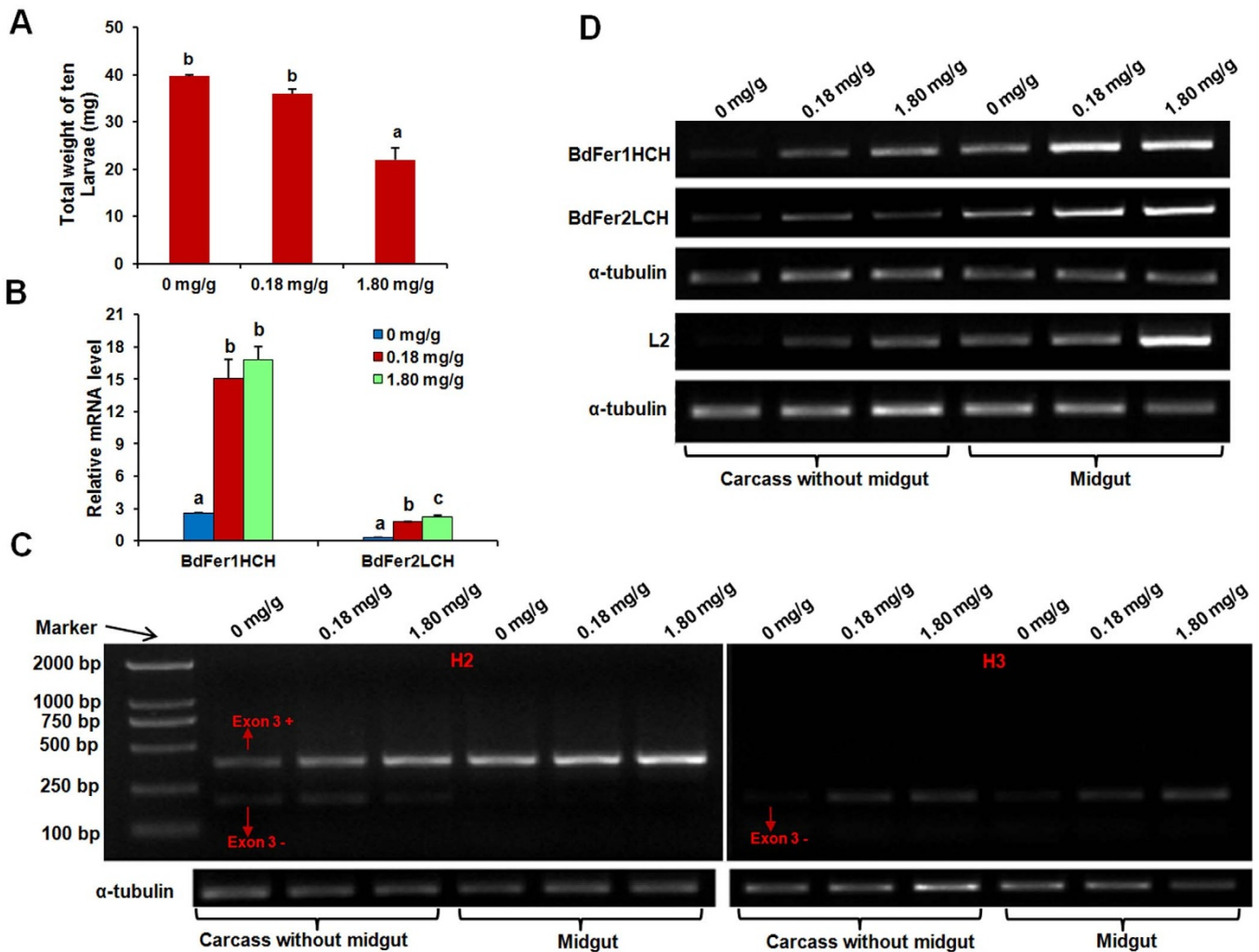
Figure 5 | Effect of iron overload on larval weight gain and ferritin expression levels in *Bactrocera dorsalis*. (A) Total weight of 10 larvae after feeding on a diet supplemented with 0 mg/g, 0.18 mg/g, or 1.80 mg/g $FeCl_3$ for 24 h. Data were analyzed by one-way ANOVA. Bars with different letters had significant differences. ($p < 0.05$, Tukey HSD's test).(B) Relative expression levels of *BdFer1HCH* and *BdFer2LCH* after iron feeding for 24 h. Bars with different letters had significant differences. ($p < 0.05$, Tukey HSD's test). (C) RT-PCR assay of the variants initiating with H-TSS2 or H-TSS3 in the midgut and carcass without midgut of larvae after iron overload for 24 h. (D) RT-PCR assay of the expression levels of all *BdFer1HCH* and *BdFer2LCH* variants, and the variant initiating with L-TSS2. *α-tubulin* was used as the loading control to indicate equal amount of RNA. The signs "+" and "−"indicate the inclusion or exclusion of alternative exons. All gels were run under the same conditions. Full length gels are shown in the supplementary data section.

levels[7]. An IRE/IRP system regulates the expression of the Fer1HCH subunit in *D. melanogaster*[5], whereas the regulatory mechanism for Fer2LCH subunit remains unknown[7]. Additionally, studies on *D. melanogaster* demonstrated that a constant ratio of Fer1HCH and Fer2LCH subunits was required for ferritin expression, and was secured by an unknown post-transcriptional mechanism[9,10], which may be conserved within dipterans. Here, for the first time, we present a possible mechanism, named intron retention, to regulate the level of LCH subunits in *B. dorsalis*. The LCH variant including exon C, which is generated by intron retention, was detected in all developmental stages of *B. dorsalis*. The inclusion of exon C introduces a premature stop codon into the transcripts and leads to the production of truncated proteins. Nonetheless, whether such truncated proteins are functional remains to be determined.

Alternative splicing events have also been reported in *LCH* genes, but only at the 5′ UTR[19]. Additionally, the exclusion of exon C only occurs when the transcripts initiate with L-TSS1 but not L-TSS2, indicating coordinating regulation by transcriptional and post-transcriptional mechanisms. Thus, alternative promoters and alternative splicing cooperate to control the levels of the BdFer2LCH subunit.

Intriguingly, like *Fer1HCH*, *BdFer1HCH* also gained an IRE in an alternatively spliced exon at the 5′ UTR[20,21]. However, the inclusion of exon 3 only occurs when the transcripts initiate with H-TSS2. Thus, BdFer1HCH levels are jointly regulated by alternative promoters and alternative splicing, which has not previously been reported in other insect homologues. Based on the highly similar genomic structures among ferritin genes[7], similar mechanisms may also exist in other insects.

The tight clustering of the secreted ferritin genes allows for their coordinated regulation at their transcriptional levels and accounted, to some extent, for their similar transcriptional profiles[8,21–23]. Such a clustering structure is also conserved in *B. dorsalis* ferritin genes, which may explain why the tissue and developmental expression profiles of *BdFer1HCH* and *BdFer2LCH* are quite similar. The genetic structures of *BdFer1HCH* and *BdFer2LCH* are most similar to that of *D. melanogaster* ferritin[7]. Analysis of the control region implies that *BdFer1HCH* and *BdFer2LCH* may share some regulatory elements. Despite the transcriptional similarity between *BdFer1HCH* and *BdFer2LCH*, *BdFer2LCH* has distinctly higher expression in female adults than in other developmental stages, unlike
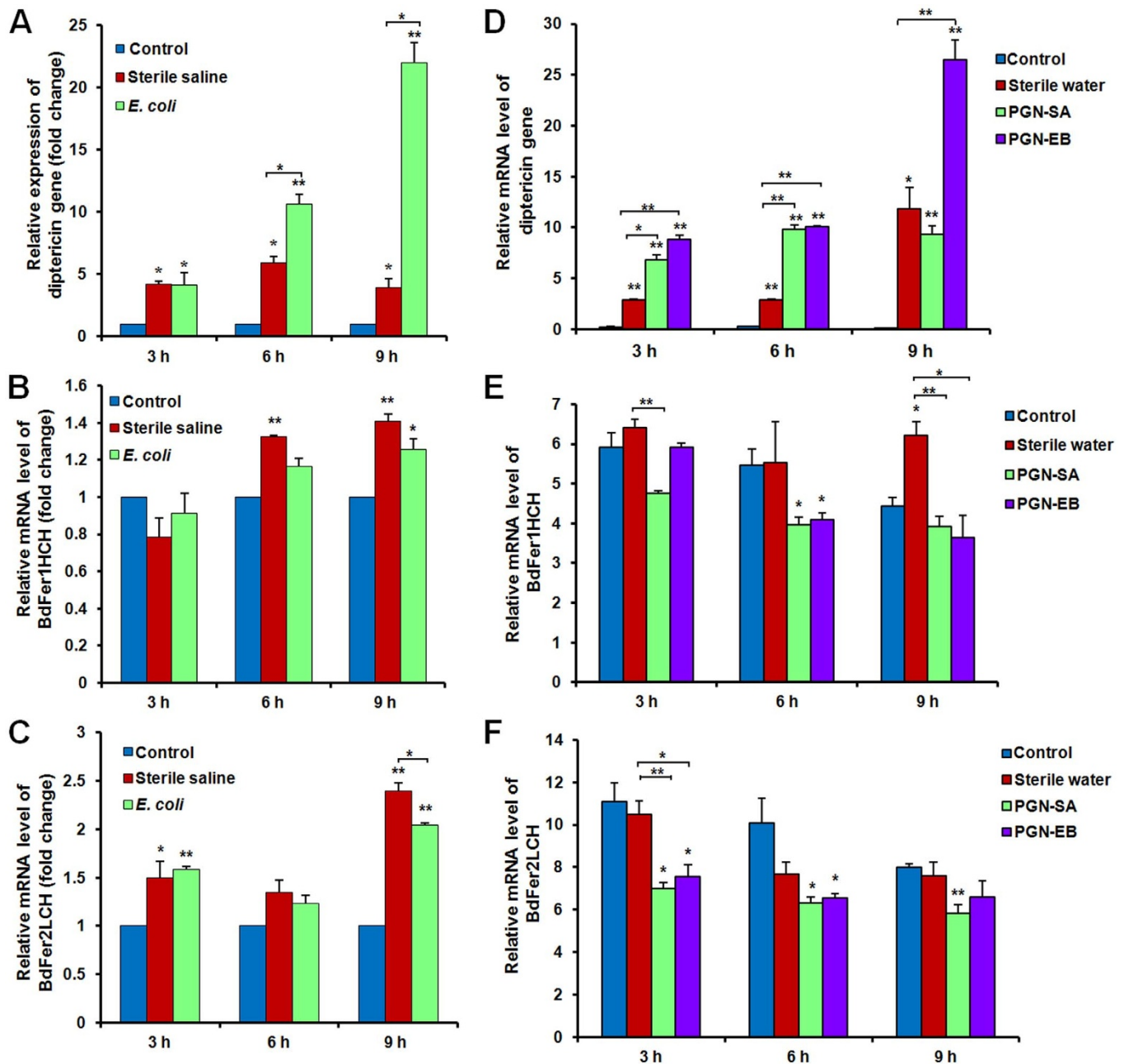
Figure 6 | Effects of *Escherichia coli*, PGN-SA, and PGN-EB challenge on the mRNA levels of antimicrobial peptide gene *diptericin* (A, D), *BdFer1HCH* (B, E), and *BdFer2LCH* (C, F). (A, B, C) Relative expression levels of *diptericin*, *BdFer1HCH*, and *BdFer2LCH* after *E. coli* challenge. All values were normalized relative to the control group (set as 1). Data represent mean $2^{-\Delta\Delta Ct}$ values of three independent biological replicates ± SEM. (D, E, F) Relative expression levels of *diptericin*, *BdFer1HCH*, and *BdFer2LCH* after PGN-SA and PGN-EB challenge. Results are represented as the mean $2^{-\Delta Ct}$ values of three independent biological replicates ± SEM. The two-tailed, unpaired t-test was used to test significance. Asterisks indicate significant differences in relative expression. (*, $p < 0.05$; **, $p < 0.01$).

BdFer1HCH. Such variation may imply an extra role for *BdFer2LCH* in female adults, which remains to be further characterized.

Iron overload can dramatically alter the abundance of ferritin transcripts and alter the mRNA types[21,23,24]. Here, we confirmed that the transcript abundance was dramatically altered by iron overload. A high dose of FeCl₃ can significantly retard the growth of *B. dorsalis* larvae, while low doses may cause small amounts of weight gain. Interestingly, although the expressions of both *BdFer1HCH* and *BdFer2LCH* were up-regulated by iron overload, no apparent dose effect was observed, which may be explained by the high storage capacity of the ferritin protein and reduced absorption of iron in the midgut[5,15]. Expression was up-regulated not only in the midgut,

but also in other tissues, suggesting a role for ferritins in iron transport and iron detoxification. Previously, a study on *Fer1HCH* indicated that a functional IRE was present only at the 5′ UTR of certain splice variants, which were preferentially encoded under iron-limiting conditions[21]. By contrast, in *B. dorsalis*, the transcripts containing IRE dominated at all developmental stages and in all tissues, and were preferentially up-regulated by iron overload. Moreover, in the larval midgut, the variants including IRE were the main mRNA types. Hence, we can infer that *BdFer1HCH* may prefer an adjustable form, which may allow *B. dorsalis* to adjust to changing iron conditions. However, more research is needed to explain the differences among ferritins in different insect species.

The BR-C gene is a primary response gene in the ecdysteroids signaling pathway, and encodes four BR-C isoforms (Z1–Z4) in *D. melanogaster*. These isoforms are involved in a number of insect physiological processes, such as metamorphosis, oogenesis, and vitellogenesis[25]. Accordingly, the distribution of BR-C binding elements in the upstream control region is evidence that *B. dorsalis* ferritin may be responsive to 20E. The immediate induction of *BdFer1HCH* and *BdFer2LCH* by 20E injection corroborates our hypothesis that the expression of *B. dorsalis* ferritin is regulated by hormone level. Additionally, the similar expression patterns of *BdFer1HCH* and *BdFer2LCH* under 20E regulation may be attributed to the shared 20E-responsive transcription factor binding elements in the control region. The regulation of ferritin expression by 20E has never been reported, whereas ecdysteroids have been demonstrated to regulate the expression of the *Apis mellifera* transferrin gene[26]. Hence, ecdysteroids can regulate free iron levels by regulating the expression of iron-binding proteins, which further suggests that a certain iron level is required for hormone regulation. Additionally, some components in the ecdysteroidogenic and the signaling pathways require iron[27,28], so their protein activities are subject to the iron level. Accordingly, 20E is probably capable of regulating its own level and its signal transduction by controlling the iron level.

Significant transcriptional regulation of ferritins by bacterial infection has been reported in insects[29–31]. However, the actual regulation mechanisms by which bacterial infection regulates ferritin remain unclear. The host recognizes the bacteria by sensing specific forms of Peptidoglycan (PGN) via peptidoglycan recognition proteins (PGRPs)[32]. Differential immune effects are stimulated by Gram-negative and Gram-positive bacteria because of the differences in their PGNs[32]. The antimicrobial peptide (AMP) diptericin is very active against Gram-negative bacteria and is generated by the IMD pathway[32]. The identification of putative NF-κB binding sites in the first intron sequences downstream from the start codon indicated that *B. dorsalis* ferritin may also participate in immune defense. Thus, we examine the transcriptional responses of ferritins to *E. coli*, PGN-SA, and PGN-EB.

Significant up-regulation of the *diptericin* gene was observed post-treatment, demonstrating an acute immune reaction of *B. dorsalis* to *E. coli*, PGN-SA, and PGN-EB. Additionally, the more intense induction by *E. coli* and PGN-EB than by PGN-SA confirmed that the IMD pathway is activated by Gram-negative bacteria or DAP-type peptidoglycans. However, both *BdFer1HCH* and *BdFer2LCH* were down-regulated by *E. coli*, PGN-SA, and PGN-EB exposure, as in *Anopheles gambiae*[30]. Apparently, two distinct strategies, iron-withholding and the production of reactive oxygen species (ROS), are used by different insects to defend against microorganisms by regulating the free iron levels. Iron is an essential nutrient for pathogens[33,34], and iron-withholding is an innate immune mechanism in hosts[4,35]. Hence, ferritins may act as immune effectors by sequestering extra iron to limit its availability to the pathogens. Meanwhile, excessive free iron can also lead to the production of ROS, which are harmful to microorganisms[36,37]; therefore, the host can increase the amount of free iron by reducing the expression levels of ferritins. This strategy may work in *B. dorsalis* to resist invading microorganisms, because ferritin expression was repressed by *E. coli*, PGN-SA, and PGN-EB. However, more evidence is needed to determine whether such defensive strategies are really used by the host insects.

This study provides an initial understanding of a regulatory mechanism used by *B. dorsalis* to control the LCH subunit levels through generating truncated proteins, which result from the coordination of alternative promoters and intron retention. The presence of IRE at the 5′ UTR of *BdFer1HCH* could also be attributed to the coordination of alternative promoters and alternative splicing; the variants, including IRE, were the main mRNA type and induced by iron overload, which is contrary to the case in *D. melanogaster*.

Additionally, we also show that *B. dorsalis* ferritin could be induced by 20E and immune challenges.

Methods

Insect rearing and sample preparation. The stock colony of *B. dorsalis* was originally collected from Fujian Province, China. Insects were maintained under constant temperature at $27 \pm 1°C$, $75 \pm 5\%$ relative humidity, and a photoperiod cycle of $14:10$ h light:dark. Insects were reared as previously described[38].

Samples including eggs, 1–8-day-old larvae, 1–10-day-old pupae, and 1–19-day-old female adults were collected at 3-day intervals. In the tissue-specific experiment, 5-day-old larvae and 5–6-day-old adults were used for tissue isolation. The insects were dissected individually in saline solution using dissecting needles under a microscope (Olympus SZX12, Tokyo, Japan). Larval tissues, including the fat body, integument, midgut, Malpighian tubules, and trachea, and adult tissues including head (without antennae), thorax (without legs), antennae, legs, fat body, midgut, Malpighian tubules, ovary, and testis, were collected. All tissue samples were stored in RNAstore Reagent (Tiangen Biotech, Beijing, China) at $-80°C$ until used for RNA extraction. Three replicates were run per sample.

Iron overload, 20E injection, and immune challenge. Three-day-old larvae with similar body sizes were starved overnight. Then, three sets of 45 individual larvae were transferred into a Petri dish (diameter: 6 cm) filled with 19 g artificial diet supplemented with $FeCl_3$ (dissolved in 1 mL saline) at a final concentration of 1.8 mg/g or 0.18 mg/g. For the control group, 45 larvae were transferred onto a Petri dish filled with 19 g artificial diet supplemented with 1 mL saline only. Ten larvae were randomly sampled from each group after 24 h and weighed. To analyze the expression profile, five larvae were sampled from each group 12, 24, and 36 h after the beginning of feeding. The larval midgut and the remaining carcass at 24 h were dissected individually in saline and stored in RNAstore Reagent. About 5 mg of midgut were collected as one sample. The carcasses without midgut from five individuals were used as one sample.

Two milligrams of 20 E (Fluorochem Ltd, Glossop, UK) were diluted into 400 μL distilled deionized (DD) water at a final concentration of 5 μg/mL. Five-day-old larvae were injected at a dose of 0.5 μg/larva using a nano-injector (Nanoject II, Drummond Scientific, Broomall, PA, USA) as the treatment group. The control group was injected with an equivalent volume of DD water. Five individual larvae were randomly sampled from each group 1, 4, 8, and 12 h post injection.

For the immune challenge, *E. coli* (Trans5α chemically competent cells) was pre-cultured in LB medium. Stationary-phase cells were collected by centrifugation at $6000 \times g$ for 1 min, washed three times, and finally suspended in sterilized saline solution. Four-day-old larvae were injected with 69 nL bacteria solution ($OD_{600} = 2.1$) through the inter-segmental membrane for the *E. coli* group, or injected with 69 nL sterilized saline for the saline group. The control group was handled the same way but without injection. Five individual larvae were randomly collected from each group 3, 6, and 9 h post injection. PGN-SA (peptidoglycan from *S. aureus*; InvivoGen, San Diego, CA, USA) and PGN-EB (peptidoglycan from *E. coli 0111:B4*; InvivoGen) were diluted into sterilized water at final concentrations of 1.0 mg/mL. Four-day-old larvae were injected with 2×69 nL PGN-SA solution, PGN-EB solution or sterilized water. The control group was handled the same way but without injection. Five individual larvae were randomly collected from each group 3, 6, and 9 h post injection.

Each of the above-mentioned treatments was performed in triplicate. Three replicates were collected for each sample. All samples were stored at $-80°C$ until used for total RNA extraction.

RNA isolation and cDNA synthesis. Total RNA from tissues (5 mg) was isolated using RNeasy® Plus Micro Kit (Qiagen GmbH, Hilden, Germany) according to the manufacturer's instructions. Total RNA from other samples was extracted using TRIzol® reagent (Invitrogen, Carlsbad, CA, USA), with an additional digestion step using RQ1 RNase-Free DNase (Promega, Madison, WI, USA) to digest the genomic DNA. The quality, purity, and concentration of RNA were measured at 260 nm and 280 nm using a NanoVue UV-Vis spectrophotometer (GE Healthcare Bio-sciences, Uppsala, Sweden), and RNA integrity was checked by 1.0% agarose gel electrophoresis. For first strand cDNA synthesis, 500 ng of total RNA was reverse transcribed using the PrimeScript 1st Strand cDNA Synthesis Kit (Takara, Dalian, China) with random hexamer and oligo (dT) primers, according to the manufacturer's instructions.

cDNA and genomic sequence cloning. Based on the transcriptomic data of the *B. dorsalis* larval midgut[36], the ORFs were identified. To determine the UTRs, rapid amplification of cDNA ends (RACE) was performed using the SMARTer RACE cDNA Amplification Kit (Clontech, Mountain View, CA, USA) according to the manufacturer's instructions. To determine the genetic structure, *B. dorsalis* genomic DNA was extracted from a female adult using a Tissue/Cell gDNA Mini Kit (Watson Biotechnologies, Shanghai, China) following the manufacturer's protocols. All PCRs were carried out in a C1000TM Thermal Cycler (Bio-Rad, Hercules, CA, USA) in 25 μL reaction mixtures containing 1 μL template cDNA/genomic DNA, 2.5 μL 10 × PCR buffer (Mg2+ free), 2.5 μL Mg2+ (25 mM), 2.0 μL dNTPs (2.5 mM each), 1 μL of each primer (10 μM), and 0.25 μL rTaq (5 U/μL) (TaKaRa). PCR was carried out as follows: one cycle at 94°C for 1 min; 30 cycles at 94°C for 30 s, 60°C for 30 s, and 72°C for 1 min; one cycle of 72°C for 5 min and holding at 16°C. All primers are

listed in Supplementary Table 1. All PCR products were cloned into the pGEM-T Easy vector (Promega) and transformed into Trans5α chemically competent cells (Transgen, Beijing, China). Three clones for each PCR product were randomly selected for sequencing (BGI, Shenzhen, China).

Sequence analysis. The SignalP 4.1 server was used to predict the signal peptide[39]. N-Glycosylation sites were predicted by the NetNGlyc 1.0 server[40]. To identify putative TFBSs in the control regions, we used the program AliBaba 2.1 provided by TESS (Transcription Element Search System) (http://www.gene-regulation.com/pub/programs/alibaba2/index.html) and an online server TFSEARCH [Searching Transcription Factor Binding Sites (ver. 1.3)] (http://www.cbrc.jp/research/db/TFSEARCH.html).

Reverse transcriptase polymerase chain reactions (RT-PCR) analysis. RT-PCR was performed to indicate the relative expression levels of the variants. PCR conditions and procedures were as described above. Primers are listed in Supplementary Table 2. Each PCR product (10 μL) was analyzed by 2.0% agarose gel electrophoresis with GoldView II (Solarbio Co., Ltd., Shanghai, China) staining. The gel was imaged using a Gel Doc XR System (Bio-Rad) and analyzed using Quantity One software (version 4.6.7; Bio-Rad). All electrophoresis images were refined using Adobe Photoshop CS5 (Adobe Systems, San Jose, CA, USA). Three replicates were performed for each trial.

Real-time quantitative polymerase chain reactions (RT-qPCR). The efficiency and determination coefficient (R^2) of PCR amplification were calculated from the slope of the standard curve determined from five serial dilutions of one cDNA sample. Primers are listed in Supplementary Table 3. Each reaction was performed within the StepOne Plus Real-Time PCR System (Applied Biosystems, Carlsbad, CA, USA) in a 20 μL volume containing 1 μL cDNA template, 10 μL iQ SYBR Green Supermix (Bio-Rad), 0.2 μL of CXR reference dye, 1 μL of each primer (10 μM), and 6.8 μL of nuclease-free water. The reaction conditions were: one cycle at 95°C for 2 min, followed by 40 cycles at 95°C for 15 s and 60°C for 30 s. Melting curve analysis from 60°C to 95°C was applied to all reactions to ensure specificity and consistency of all generated products.

Validation of stable reference genes under iron overload and bacterial challenge. We validated eight candidate reference genes (Supplementary Table 4) under iron overload and immune challenge conditions. The primers were derived from a previous study (Supplementary Table 3)[41]. All data were analyzed by the tool RelFinder (http://www.leonxie.com/referencegene.php), which integrated the current major computational programs including geNorm[42], Normfinder[43], BestKeeper[44], and the comparative Delta Ct method[45].

Data analysis. Relative expression levels were determined using the $2^{-\Delta\Delta Ct}$ or $2^{-\Delta Ct}$ method[46]. The relative expression levels at various developmental stages were normalized to that of 18S ribosomal RNA[47]. α-tubulin was used to normalize the data of tissue expression[48] and expression under 20E treatment[49]. Expression differences were determined using one-way analysis of variance (ANOVA) or two-tailed, unpaired t-test within SPSS 20.0 (IBM Corp, Chicago, IL, USA). All pairwise comparisons were considered to be significant when $p < 0.05$. All experiments were conducted in triplicate, and data for a given variable were analyzed at the same time.

1. Andrews, N. C. Forging a field: the golden age of iron biology. *Blood* **112**, 219–230 (2008).
2. Hower, V. *et al.* A general map of iron metabolism and tissue-specific subnetworks. *Mol Biosyst* **5**, 422–443 (2009).
3. Kell, D. B. Iron behaving badly: inappropriate iron chelation as a major contributor to the aetiology of vascular and other progressive inflammatory and degenerative diseases. *BMC Med Genomics* **2**, 2 (2009).
4. Weinberg, E. D. & Miklossy, J. Iron withholding: A defense against disease. *J. Alzheimers Dis.* **13**, 451–463 (2008).
5. Nichol, H., Law, J. H. & Winzerling, J. J. Iron metabolism in insects. *Ann Rev Entomol* **47**, 535–559 (2002).
6. Hamburger, A. E., West, Jr. A. P., Hamburger, Z. A., Hamburger, P. & Bjorkman, P. J. Crystal structure of a secreted insect ferritin reveals a symmetrical arrangement of heavy and light chains. *J Mol Biol* **349**, 558–569 (2005).
7. Dunkov, B. & Georgieva, T. Insect iron binding proteins: Insights from the genomes. *Insect Biochem Mol Biol* **36**, 300–309 (2006).
8. Pham, D. D. & Chavez, C. The ferritin light-chain homologue promoter in *Aedes aegypti. Insect Mol Biol* **14**, 263–270 (2005).
9. Missirlis, F. *et al.* Homeostatic mechanisms for iron storage revealed by genetic manipulations and live imaging of *Drosophila* ferritin. *Genetics.* **177**, 89–100 (2007).
10. Tang, X. & Zhou, B. Ferritin is the key to dietary iron absorption and tissue iron detoxification in *Drosophila melanogaster. FASEB J* **27**, 288–298 (2013).
11. Bonnett, T. R. *et al.* Global and comparative proteomic profiling of overwintering and developing mountain pine beetle, *Dendroctonus ponderosae* (Coleoptera: Curculionidae), larvae. *Insect Biochem Mol Biol* **42**, 890–901 (2012).
12. Colinet, H., Overgaard, J., Com, E. & Sørensen, J. G. Proteomic profiling of thermal acclimation in *Drosophila melanogaster. Insect Biochem Mol Biol* **43**, 352–365 (2013).
13. Gutierrez, L. *et al.* Biophysical and genetic analysis of iron partitioning and ferritin function in *Drosophila melanogaster. Metallomics* **5**, 997–1005 (2013).
14. Mahadav, A., Kontsedalov, S., Czosnek, H. & Ghanim, M. Thermotolerance and gene expression following heat stress in the whitefly *Bemisia tabaci* B and Q biotypes. *Insect Biochem Mol Biol* **39**, 668–676 (2009).
15. Pham, D. Q. D. & Winzerling, J. J. Insect ferritins: Typical or atypical? *BBA-Gen Subjects* **1800**, 824–833 (2010).
16. Li, S. Identification of iron-loaded ferritin as an essential mitogen for cell proliferation and postembryonic development in *Drosophila. Cell Res* **20**, 1148–1157 (2010).
17. Clarke, A. R. *et al.* Invasive phytophagous pests arising through a recent tropical evolutionary radiation: the *Bactrocera dorsalis* complex of fruit flies. *Ann Rev Entomol* **50**, 293–319 (2005).
18. Jin, T., Zeng, L., Lin, Y., Lu, Y. & Liang, G. Insecticide resistance of the oriental fruit fly, *Bactrocera dorsalis* (Hendel)(Diptera: Tephritidae), in mainland China. *Pest Manag Sci* **67**, 370–376 (2011).
19. Geiser, D. L., Chavez, C. A., Flores-Munguia, R., Winzerling, J. J. & Pham, D. Q. D. *Aedes aegypti* ferritin. *Eur J Biochem* **270**, 3667–3674 (2003).
20. Lind, M. I., Ekengren, S., Melefors, Ö. & Söderhäll, K. *Drosophila* ferritin mRNA: alternative RNA splicing regulates the presence of the iron-responsive element. *FEBS Lett* **436**, 476–482 (1998).
21. Georgieva, T., Dunkov, B. C., Harizanova, N., Ralchev, K. & Law, J. H. Iron availability dramatically alters the distribution of ferritin subunit messages in *Drosophila melanogaster. Proc Natl Acad Sci* **96**, 2716–2721 (1999).
22. Georgieva, T., Dunkov, B., Law, J., Dimopoulos, G. & Kafatos, F. *Anopheles gambia* secreted ferritin: characterization of cDNAs encoding two subunits, mRNA expression patterns, and gene organization. Abstract of the Fourth International Symposium on Molecular Insect Science. *J Insect Sci* **2**, 17 (2002).
23. Georgieva, T., Dunkov, B. C., Dimov, S., Ralchev, K. & Law, J. H. *Drosophila melanogaster* ferritin: cDNA encoding a light chain homologue, temporal and tissue specific expression of both subunit types. *Insect Biochem Mol Biol* **32**, 295–302 (2002).
24. Dunkov, B. C., Georgieva, T., Yoshiga, T., Hall, M. & Law, J. H. Aedes aegypti ferritin heavy chain homologue: feeding of iron or blood influences message levels, lengths and subunit abundance. *J Insect Sci* **2**, 7 (2002).
25. Piulachs, M. D., Pagone, V. & Bellés, X. Key roles of the Broad-Complex gene in insect embryogenesis. *Insect Biochem Mol Biol* **40**, 468–475 (2010).
26. do Nascimento, A. M., Cuvillier-Hot, V., Barchuk, A. R., Simões, Z. L. P. & Hartfelder, K. Honey bee (*Apis mellifera*) transferrin-gene structure and the role of ecdysteroids in the developmental regulation of its expression. *Insect Biochem Mol Biol* **34**, 415–424 (2004).
27. Warren, J. T. *et al.* Molecular and biochemical characterization of two P450 enzymes in the ecdysteroidogenic pathway of *Drosophila melanogaster. Proc Natl Acad Sci* **99**, 11043–11048 (2002).
28. Reinking, J. *et al.* The *Drosophila* nuclear receptor E75 contains heme and is gas responsive. *Cell* **122**, 195–207 (2005).
29. Altincicek, B., Knorr, E. & Vilcinskas, A. Beetle immunity: Identification of immune-inducible genes from the model insect *Tribolium castaneum. Dev Comp Immunol* **32**, 585–595 (2008).
30. Paskewitz, S. M. & Shi, L. The hemolymph proteome of *Anopheles gambiae. Insect Biochem Mol Biol* **35**, 815–824 (2005).
31. Wang, D. *et al.* Molecular characterization of iron binding proteins, transferrin and ferritin heavy chain subunit, from the bumblebee *Bombus ignitus. Comp Biochem Physiol B* **152**, 20–27 (2009).
32. Lemaitre, B. & Hoffmann, J. The host defense of *Drosophila melanogaster. Annu Rev Immunol* **25**, 697–743 (2007).
33. Nappi, A. J. & Vass, E. Iron, metalloenzymes and cytotoxic reactions. *Cell Mol Biol* **46**, 637–647 (2000).
34. Yoshiga, T. *et al. Drosophila melanogaster* transferrin. *Eur J Biochem* **260**, 414–420 (1999).
35. Wang, L. & Cherayil, B. J. Ironing out the wrinkles in host defense: interactions between iron homeostasis and innate immunity. *J Innate Immun* **1**, 455–464 (2009).
36. Hentze, M. W. & Kühn, L. C. Molecular control of vertebrate iron metabolism: mRNA-based regulatory circuits operated by iron, nitric oxide, and oxidative stress. *Proc Natl Acad Sci* **93**, 8175–8182 (1996).
37. Baker, H. M., Anderson, B. F. & Baker, E. N. Dealing with iron: common structural principles in proteins that transport iron and heme. *Proc Natl Acad Sci* **100**, 3579–3583 (2003).
38. Shen, G. M. *et al.* In silico cloning and annotation of genes involved in the digestion, detoxification and RNA interference mechanism in the midgut of *Bactrocera dorsalis* [Hendel (Diptera: Tephritidae)]. *Insect Mol Biol* **4**, 354–365 (2013).
39. Petersen, T. N., Brunak, S., von Heijne, G. & Nielsen, H. SignalP 4.0: discriminating signal peptides from transmembrane regions. *Nat Methods* **8**, 785–786 (2011).
40. Gupta, R., Jung, E. & Brunak, S. Prediction of N-glycosylation sites in human proteins. http://www.cbs.dtu.dk/services/NetNGlyc/ (2004) Date of access: 5th, Sep., 2013.
41. Shen, G. M., Huang, Y., Jiang, X. Z., Dou, W. & Wang, J. J. Effect of β-cypermethrin Exposure on the stability of nine housekeeping genes in *Bactrocera dorsalis* (Diptera: Tephritidae). *Flo Entomol* **96**, 442–450 (2013).

42. Vandesompele, J. *et al.* Accurate normalization of real-time quantitative RT-PCR data by geometric averaging of multiple internal control genes. *Genome Biol* **3**, research0034 (2002).

43. Andersen, C. L., Jensen, J. L. & Ørntoft, T. F. Normalization of real-time quantitative reverse transcription-PCR data: a model-based variance estimation approach to identify genes suited for normalization, applied to bladder and colon cancer data sets. *Cancer Res* **64**, 5245–5250 (2004).

44. Pfaffl, M. W., Tichopad, A., Prgomet, C. & Neuvians, T. P. Determination of stable housekeeping genes, differentially regulated target genes and sample integrity: BestKeeper–Excel-based tool using pair-wise correlations. *Biotech Lett* **26**, 509–515 (2004).

45. Silver, N., Best, S., Jiang, J. & Thein, S. L. Selection of housekeeping genes for gene expression studies in human reticulocytes using real-time PCR. *BMC Mol Biol* **7**, 33 (2006).

46. Livak, K. J. & Schmittgen, T. D. Analysis of Relative Gene Expression Data Using Real-Time Quantitative PCR and the $2^{-\Delta\Delta CT}$ Method. *Methods* **25**, 402–408 (2001).

47. Shen, G. M., Wang, X. N., Dou, W. & Wang, J. J. Biochemical and molecular characterisation of acetylcholinesterase in four field populations of *Bactrocera dorsalis* (Hendel)(Diptera: Tephritidae). *Pest Manag Sci* **68**, 1553–1563 (2012).

48. Shen, G. M., Jiang, H. B., Wang, X. N. & Wang, J. J. Evaluation of endogenous references for gene expression profiling in different tissues of the oriental fruit fly *Bactrocera dorsalis* (Diptera: Tephritidae). *BMC Mol Biol* **11**, 76 (2010).

49. Yang, W. J., Xu, K. K., Cong, L. & Wang, J. J. Identification, mRNA Expression, and functional analysis of Chitin Synthase 1 gene and its two alternative splicing variants in oriental fruit fly, *Bactrocera dorsalis*. *Int J Biol Sci* **9**, 331 (2013).

Acknowledgments

Author contributions

J.J.W. and X.Z.J. designed this project and experiments. X.Z.J. and L.C. performed the experiments. X.Z.J., J.Z.N. and W.D. completed the figures and tables. X.Z.J. and J.J.W. analyzed the data and wrote the manuscript.

Additional information

Supplementary information accompanies this paper at http://www.nature.com/scientificreports

Competing financial interests: The authors declare no competing financial interests.

How to cite this article: Jiang, X.-Z., Cong, L., Niu, J.-Z., Dou, W. & Wang, J.-J. Alternative splicing contributes to the coordinated regulation of ferritin subunit levels in *Bactrocera dorsalis* (Hendel). *Sci. Rep.* **4**, 4806; DOI:10.1038/srep04806 (2014).